Available online at www.sciencedirect.com
ScienceDirect
Journal of Magnetic Resonance 192 (2008) 1–7
JMR Journal of Magnetic Resonance
www.elsevier.com/locate/jmr

Surface UV aging of elastomers investigated with microscopic resolution by single-sided NMR

N.O. Goga [a], D.E. Demco [a,b], J. Kolz [a], R. Ferencz [a], A. Haber [a], F. Casanova [a], B. Blümich [a,*]

[a] *Institute for Technical and Macromolecular Chemistry, RWTH Aachen University, Worringerweg 1, D-52072 Aachen, Germany*
[b] *Technical University Cluj-Napoca, str. Daicoviciu 15, 400020 Cluj-Napoca, Romania*

Received 25 August 2007; revised 27 October 2007
Available online 19 November 2007

Abstract

Depth profiles taken from the surface of UV irradiated natural rubber sheets have been measured with microscopic resolution using a Profile NMR-MOUSE®. An NMR observable related to the sum of the spin echoes in the Carr–Purcell–Meiboom–Gill pulse sequence was used to characterize the cross-link density changes produced by the action of UV radiation in each sheet. The aging process was investigated as function of irradiation time and penetration depth. An exponential attenuation law with a space dependent absorption coefficient describes the change in the NMR observable with penetration depth. An Avrami model is used to describe the dependence of the absorption coefficient on the aging time. The method can be applied to investigate the effect of various aging agents on the surfaces of elastomers.

Keywords: ^{1}H NMR; Transverse magnetization relaxation; NMR-MOUSE; Elastomers; UV aging

1. Introduction

The effect of UV light on polymers, and especially on elastomers is still not completely understood, although extensive data have been reported on the action of electromagnetic radiation on such materials [1–3]. Studying the interaction of UV irradiation with elastomer networks is an important topic in polymer science relevant to the polymer industry.

The interest in the transformation of organic polymers under the action of UV radiation relates to a number of reasons. First, polymer modification by ionizing radiation is an important technological means for functionalizing polymer surfaces [4]. The reaction mechanism is complex and involves the action of many primary particles. Second, an analysis of this process is important considering the material deterioration during processing and use in different environmental conditions. One example is the dry etching of polymer resists in microelectronics. Small structures require high resolution and thus short wavelength light. Furthermore, for a lifetime prediction, the natural exposure to UV radiation has to be considered. The UV component of sun light deteriorates many polymeric materials especially in the presence of oxygen. Understanding the long-term aging characteristics of elastomers is critical for performance assessment and lifetime prediction of such materials.

As the irradiation enters from the outside and is absorbed by the polymer, spatial heterogeneity develops in originally homogeneous objects. For this purpose, the development of new experimental techniques that can probe the spatial heterogeneity of aged polymers is important. NMR and especially magnetic resonance imaging (MRI) are experimental techniques that *have* seen an ever-increasing role in material science, particularly in the spatial analysis of heterogeneous polymers and composites [5–10, and references therein].

* Corresponding author. Fax: +49 264 8022185.
E-mail address: buemich@mc.rwth-aachen.de (B. Blümich).

1090-7807/$ - see front matter © 2007 Elsevier Inc. All rights reserved.
doi:10.1016/j.jmr.2007.10.017

MRI has been used in the past to investigate polymer aging and degradation. Over a decade ago Blümer and Blümich reported the T_2 maps of natural rubber thermally aged in air, which clearly reveal the growth of a surface layer which hardened with the aging time [11]. MRI has also been used to investigate the biodegradation of polymer films [12], the aging in nitrile rubber elastomers [13], the degradation of rubber and polystyrene [14], the oxidative aging of natural rubber [15,16], and radiation effects in polymer gels [17]. Recently, ^{1}H relaxation encoded NMR images were measured to investigate the thermo-oxidative aging in a hydroxy-terminated polybutadiene based elastomer [18] and to establish a correlation with Young's modulus. Changes in the transverse relaxation and double-quantum buildup curves due to ^{1}H residual dipolar couplings of polymers have been correlated before with the modulus and induced stress [19–22].

In the last few years, several NMR applications have been developed which operate in strong static magnetic field gradients [23,24]. A prominent and most practical example is the development of single-sided NMR devices like the NMR-MOUSE® [25,26] with applications to non-destructive material testing of arbitrarily large objects [27–30]. For example, the orientation dependence of NMR parameters can easily be investigated with single-sided devices for large, stretched samples [29]. Furthermore, mobile, one-sided NMR imagers have been designed and applied to material investigations [24,31,32].

The NMR-MOUSE® is characterized by strong inhomogeneities of the static and radio-frequency magnetic fields. But even in the presence of these field inhomogeneities, the NMR relaxation times and parameters of translational motion can be measured by spin echo techniques [5]. There are several advantages of working with such fields. The inhomogeneous polarization field $\boldsymbol{B}_0$ provides spatial localisation along the gradient direction. Knowing the gradient profile of the sensor, the image of the investigated object can be reconstructed without spatial distortions in terms of NMR relaxation and spin density parameters. In the ideal case of a constant gradient, the image reconstruction is trivial. Then the spatial resolution is proportional to the frequency resolution determined by the excitation and acquisition bandwidths (selective pulse length and acquisition time). For frequency selective excitation it is straightforward that the gradient strength determines the spatial resolution. By using strong constant gradients, separation of spatially identical intervals is possible with microscopic resolution [24].

The aim of this work is to investigate the effect of UV radiation upon cross-linked natural rubber. A special single-sided sensor with an improved magnetic field profile, the Profile NMR-MOUSE®, was used for this purpose [24]. High resolution ^{1}H NMR depth profiles have been obtained of a rubber sample after exposure to UV radiation for several days. An NMR observable related to the sum of the spin echoes in the Carr–Purcell–Meiboom–Gill pulse sequence was used to characterize the cross-link density changes produced by the action of the UV radiation. An exponential attenuation law with a linearly space dependent absorption coefficient was proposed to describe the measured space profiles at different irradiation times.

2. Experimental

2.1. Samples, UV irradiation, and NMR measurements

The investigated elastomer sample is from commercially available natural rubber (NR) SMR10 (Malaysia). The additives were 3 phr (*p*arts-per-*h*undred-*r*ubber) ZnO and 2 phr stearic acid. The sulfur and accelerator contents were 3 phr each. The accelerator is of the standard sulfenamide type (TBBS, benzothiazyl-2-*tert*-butyl-sulfenamide). After mixing the compound in a laboratory mixer at 50 °C, the sample was vulcanized at 160 °C in a Monsanto MDR-2000-E vulcameter.

For irradiation, a 300 W Osram Ultravitalux UV lamp with an emission spectrum in the 300–400 nm wavelength range was used. The total irradiation time was 8 days. The NMR measurements were done after 5 h, 1 day, 2 days, 4 days, and 8 days of irradiation. The distance between sample and radiation source was 20 cm.

To characterize the segmental dynamics of elastomers after irradiation, a setup consisting of the Profile NMR-MOUSE® [24] and a high precision lift was used. The Profile NMR-MOUSE® has a flat sensitive volume at a fixed distance of 5 mm above its surface, and the object is positioned on top of a lift which contains the NMR-MOUSE® (Fig. 1a). The lift changes the distance between the NMR-MOUSE® and the object with a precision better than 10 μm. In this way, the sensitive volume can be shifted through the object to acquire ^{1}H NMR parameters as a function of depth into the object (Fig. 1b). In the work reported below, depth profiles were measured in increments of 20 μm at a resonance frequency of 18.1 MHz in a uniform gradient of 22.3 T/m [24].

Carr–Purcell–Meiboom–Gill decays (CPMG) were acquired in the strongly inhomogeneous magnetic field of the sensor [24] to measure the transverse NMR relaxation. The nominal 90° and 180° pulses were 20 μs, exciting a frequency bandwidth of ca. 50 kHz, and the acquisition time per echo was set to 50 μs to achieve a frequency resolution of 20 kHz per acquisition step. For each echo 25 points were detected and averaged. The data are acquired in the linear region of the static polarizing magnetic field. Given a constant field gradient of ca. 950 kHz/mm the profiles were acquired by measuring the NMR signals from slices 20 μm thick and parallel to the scanner surface. Each sample was measured in 30 steps from the surface up to a depth of 0.6 mm. The dead time of the radio-frequency setup was 30 μs. The CPMG-train consisted of echoes acquired with echo times of 130 μs. The number of scans was 256 with a repetition time of 0.5 s. The NMR experiments were performed at 23 °C with a temperature stability of ±0.1 °C.

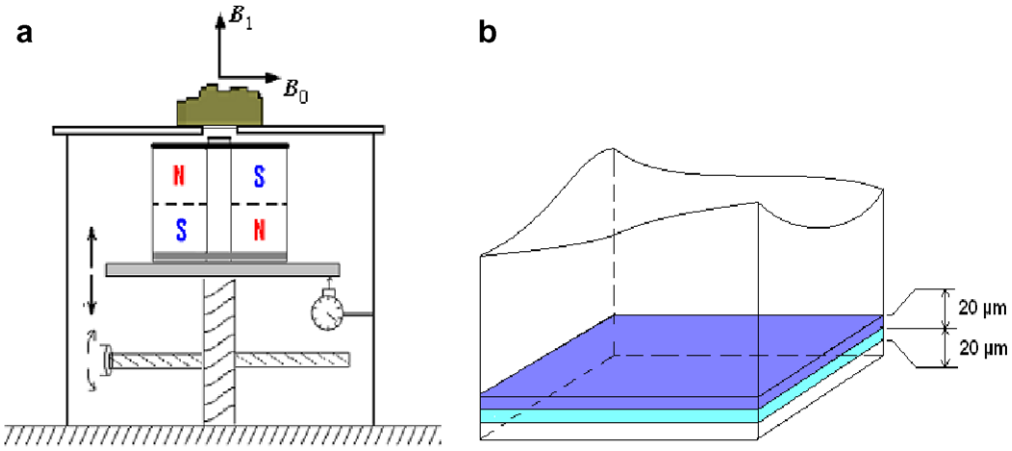

Fig. 1. (a) Experimental setup for the measurement of microscopic profiles across UV aged cross-linked NR samples. The Profile NMR-MOUSE is mounted on a high precision lift by which the distance between the NMR-MOUSE and the object on top of the lift can be changed with micrometer resolution. (b) Schematic representation of a section of the object and the sensitive volume at two positions.

Values of the effective transverse relaxation time $\overline{T}_{2\mathrm{eff}}$ were evaluated from mono-exponential fits of the CPMG echo decays. The average over the microheterogeneity of the sample is denoted by a bar. A large error in the fit with a single exponential and an improvement in the quality of the fit when fitting with a bi- or tri-exponential function revealed a multi-exponential nature of the decays (Fig. 2). However, the use of a fit function with a large number of exponentials complicates this study which is mainly focused on mapping the layer structure generated by the irradiation.

To investigate the aging process, an NMR parameter with high sensitivity towards changes in the rubber network segmental dynamics is needed, as the changes induced by UV radiation in terms of the CPMG decay are small. The NMR observable is derived from the CPMG decay and will be discussed in the next section. The normalization of the echo decays was done by division to the aver-

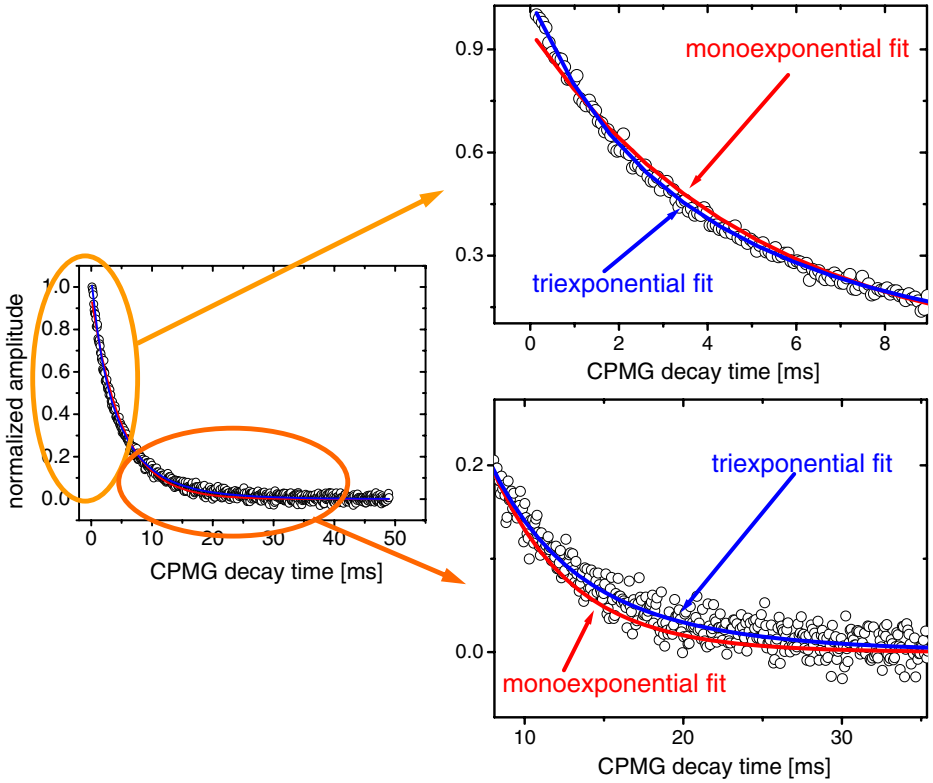

Fig. 2. Mono-exponential and tri-exponential fits of a CPMG echo decay measured in a 20 µm thick sheet of an UV aged NR sample. The zoomed sections of the decay reveal improvements in the fit when going from a mono-exponential to a tri-exponential fit.

age amplitude of the first five echoes. A summation of N_{echo} echoes increases the signal-to-noise ratio S/N by approximately:

$$\frac{S}{N} \propto \sqrt{N_{\text{echo}}}. \tag{1}$$

The first echo is excluded from summation as it is known to be lower than the second for CPMG echoes in strongly inhomogeneous fields [33].

2.2. Definition of the NMR parameter

The amplitude S_{NMR} of each point in the depth profile is derived from the envelope of the CPMG echo decay. Suppose the echo decay is described by an exponential function characterized by an average effective transverse relaxation time $\overline{T}_{2\text{eff}}$. Let us denote with S_0 the amplitude of the CPMG train extrapolated to $t = 0$ by ignoring the first echo. The sum of the echoes 2 to $N + 1$ is then given by

$$S_N = S_0 \sum_{i=1}^{N} e^{-\frac{2\tau i}{\overline{T}_{2\text{eff}}}}, \tag{2}$$

where 2τ is the echo time. We will define our NMR variable as:

$$S_{\text{NMR}} \equiv \frac{S_{\text{N}}}{S_0} = \sum_{i=1}^{N} e^{-\frac{2\tau i}{\overline{T}_{2\text{eff}}}}. \tag{3}$$

After computing the sum of N terms in the S_{NMR} above geometrical progression (Eq. (3)) we can write:

$$S_{\text{NMR}} = \frac{1 - \exp\{-2\tau N/\overline{T}_{2\text{eff}}\}}{1 - \exp\{-2\tau/\overline{T}_{2\text{eff}}\}}. \tag{4}$$

For an echo time 2τ that fulfills the condition $2\tau \ll \overline{T}_{2\text{eff}}$ we finally obtain

$$S_{\text{NMR}} \approx \frac{\overline{T}_{2\text{eff}}}{2\tau} - \frac{\overline{T}_{2\text{eff}}\left(1 - \frac{2\tau}{\overline{T}_{2\text{eff}}}\right)^N}{2\tau}. \tag{5}$$

If the condition $2\tau/\overline{T}_{2\text{eff}} \leqslant 2$ is fulfilled, the second term in the expression above is small and can be neglected, so that one can write

$$S_{\text{NMR}} \approx \frac{\overline{T}_{2\text{eff}}}{2\tau}. \tag{6}$$

In the limit of short echo time, the NMR observable is proportional to $\overline{T}_{2\text{eff}}$.

3. Results and discussion

3.1. Interaction of UV radiation with elastomers

The effect of UV irradiation on elastomers depends on the radiation energy and the irradiation time. At low radiation energy, the predominant process is photolysis characterized by a predominance of molecular hydrogen elimination. At shorter wavelengths (VUV) the radiolysis (free radical process) and photolysis give relatively similar contributions [4]. The differences consist of reactions of photo-excited singlet states of polymer molecules during photolysis while in the radiolysis the dominant contribution is given by excited triplet and ionized states.

When a polymer is irradiated with UV light, primary and secondary processes take place [4]. The primary processes are first transformations which occur when the polymer chain absorbs radiation doses exceeding its ionization energy, leading to formation of charge pairs, free charges, singlet excitation, and in much smaller amount, triplet excitation. The excited states can further decompose following either a free radical path with yields of macromolecular radicals and protons, or the molecular path when molecular hydrogen is produced with the formation of double bonds in the macromolecule. At high irradiation energies, the polymer chain can be destroyed with the formation of long chained radicals.

Rearrangements are known as secondary processes. Here the previously formed hydrogen atoms or molecules can either recombine with the macromolecules forming molecular hydrogen-radical pairs or saturating double bonds, or the unsaturated double bonds can migrate along the macromolecular backbone. In parallel, the ionization of double bonds can result in great acceleration of the decay of double bonds in the processes of intramolecular cross-linking (cyclization) and intermolecular cross-linking. Meanwhile, ionic cross-linking and physical cross-linking (entanglements) as a consequence of increased entropy are likely to occur, enhancing even more the cross-link density of the irradiated polymer.

3.2. UV aging of cross-linked natural rubber

The effect of UV radiation on cross-linked natural rubber was characterized not only as function of penetration depth but also as function of irradiation time. The main effect of the complex aging process is an increase in the cross-link density at the surface of the sample. This leads to a larger attenuation of the CPMG decays and therefore, to smaller values of our NMR observable. The position of the edge of the sample was determined by moving the NMR sensor in 20 μm increments until a NMR signal was detected. The attenuation of the radiation intensity with the penetration depth is represented by a plot of $1/S_{\text{NMR}}$ that is proportional to the effective transverse relaxation rate (Eq. (6) and Fig. 3). This NMR parameter is related linearly to the cross-link density [34].

The experimental data can be interpreted in the first approximation by considering an average attenuation coefficient $\langle\mu\rangle$ that can be evaluated based on the Beer–Lambert law. In this case the attenuation coefficient does not change with the position inside the sample but depends on the irradiation time t, i.e., $\langle\mu\rangle = \langle\mu\rangle(t)$. In the limit of the above approximation the attenuation law of the UV radiation is written as:

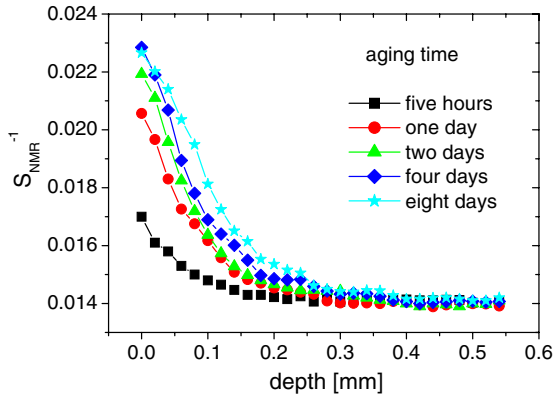

Fig. 3. Effects of UV aging versus depth for different UV irradiation times. The quantity $1/S_{NMR}$ is proportional to the reciprocal of the effective transverse relaxation time.

$$I(x) = I_0 e^{-\langle\mu\rangle x}, \tag{7}$$

where $I(x)$ is the intensity of the UV radiation at a distance x from the sample surface. The intensity of the radiation at the surface $x = 0$ is I_0.

Fitting the experimental data shown in Fig. 3 with the exponential function above, the value of $\langle\mu\rangle$ is obtained. A plot of the average attenuation coefficient versus aging time shows a decrease of $\langle\mu\rangle$ with increasing irradiation time (Fig. 4). The quasi-linear decrease of $\langle\mu\rangle$ with increasing irradiation time can be explained by the primary processes of photolysis discussed in Section 3.1. The efficiency of this process increases proportional to the irradiation time. The more chains are broken the less attenuated the incident light intensity is at a given depth x in the material. In this scenario, the secondary processes like cyclization, intermolecular cross-linking, and ionic cross-linking, which theoretically occur with high probability, seem to be neglected. Meanwhile, physical processes like entanglements (physical cross-linking) as a consequence of the higher mobility of the broken chains are likely to occur as well. Due to these complex processes the attenuation coefficient of UV radiation can depend on the intensity of the radiation and therefore on the position of the investigated sample layer from the surface.

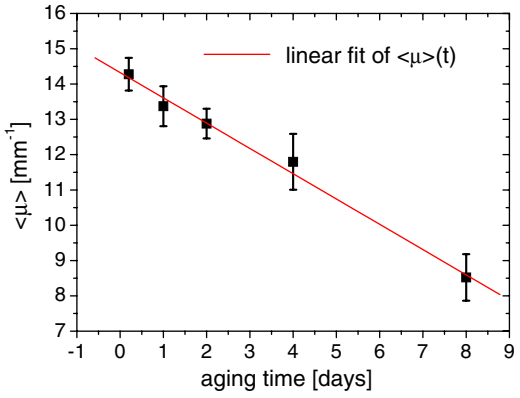

Fig. 4. Variation of the average attenuation coefficient $\langle\mu\rangle$ with the UV irradiation time (depth independent attenuation coefficient approach). The quasi-linear decrease (solid-line) of the attenuation coefficient suggests time-proportional changes of the polymer material exposed to UV irradiation.

3.3. Depth dependent radiation attenuation coefficient

When irradiating an elastomer with UV radiation, chain scissions will be induced in the polymer network. The topological constraints and cross-link density will change gradually from the network surface into the bulk. Therefore, not only the intensity $I(x)$ of UV radiation will change with the distance x from the surface but also the attenuation coefficient μ will become space dependent, i.e. $\mu = \mu(x)$. We assume that $\mu(x)$ is a quantity that exponentially decreases with the distance in the sample and write

$$\mu(x) = \mu_0 \exp\{-kx\}, \tag{8}$$

where $\mu(x)$ is the attenuation coefficient at depth x, $\mu_0 \equiv \mu(x = 0)$ is the UV absorption coefficient at the surface of our sample, and k is the spatial decay constant of the absorption coefficient. This coefficient can be correlated with supplementary cross-linking induced by the UV radiation in the polymer network. In principle, both quantities μ_0 and k are functions of the irradiation time.

The attenuation law of the UV irradiation takes into account the gradual change of electromagnetic radiation intensity with the distance. The Beer–Lambert law can be generalized for the case of a space dependent absorption coefficient, and from Eqs. (7) and (8) we have

$$\frac{dI(x)}{dx} = -\mu_0 e^{-kx} I(x), \tag{9}$$

where $I(x)$ is the intensity of the incident UV radiation at the depth x measured from the polymer network surface. The solution of Eq. (9) gives the dependence of the UV intensity $I(x)$ as a function of the penetration distance x measured from the sample surface. It has the form

$$I(x) = I_0 \exp\left\{\frac{\mu_0}{k}(e^{-kx} - 1)\right\}. \tag{10}$$

The intensity of UV radiation at the surface of the polymer network is denoted by I_0. When $kx \ll 1$, the classical law of radiation attenuation is obtained from Eq. (10), i.e., $I(x) = I_0 \exp\{-\mu_0 x\}$. For small variations of μ, the generalized attenuation law becomes $I(x) = I_0 \exp\{-\langle\mu\rangle x\}$ where $\langle\mu\rangle$ is the average value of $\mu(x)$.

The data shown in Fig. 3 represent the NMR signal as function of depth for different aging times. They were fitted with Eq. (10). These fits are shown in Fig. 5a. Fig. 5b depicts one of the experimental data sets (sample irradiated for 2 days) together with the fit function. Plots of μ_0 and k versus irradiation time are shown in Fig. 6a and b, respectively. A monotonic decrease of μ with the irradiation time is observed (Eq. (8)). The plot of μ_0 versus irradiation time (Fig. 6a) shows an increase of the attenuation coefficient at the sample surface followed by saturation after ca. 2 days of irradiation. This increase can be explained as conse-

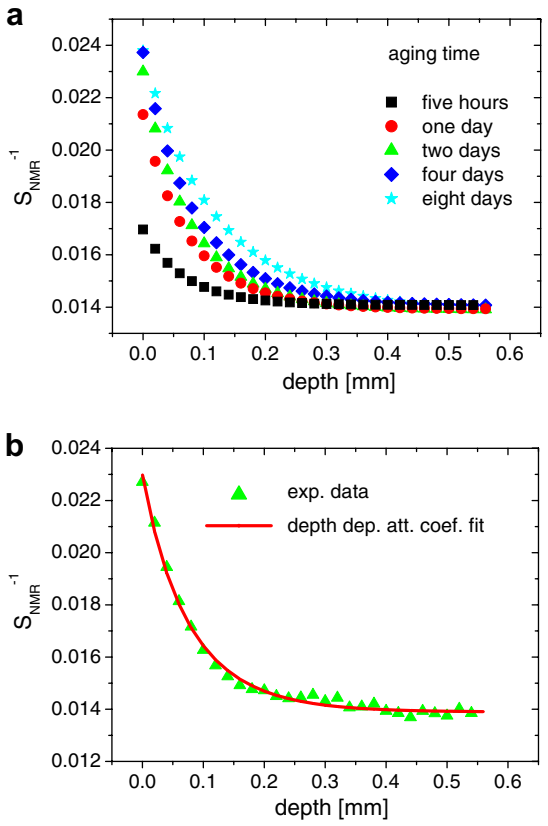

Fig. 5. (a) Fits of $1/S_{NMR}$ as function of depth for different aging times with Eq. (10). (b) One of the experimental data sets (NR UV irradiated for 2 days) together with the fit curve. The uncertainty of the fit is less than 4%.

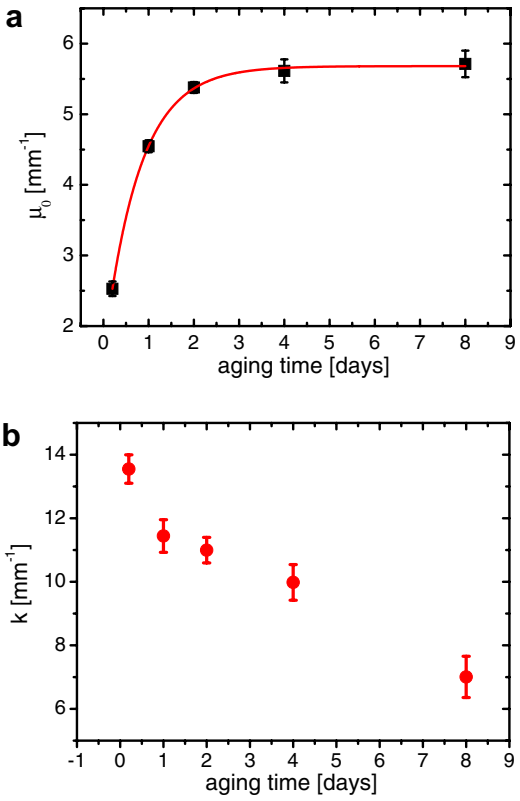

Fig. 6. (a) Plot of μ_0 versus aging time fitted with an Avrami model function. (b) Plot of k versus UV irradiation time. The plot suggests a monotonic decrease of the variation rate of μ with the irradiation time.

quence of the increasing UV radiation induced cross-link density until saturation. The decrease of the quantity k (Fig. 6b) suggests a tendency that the variation of μ with depth is reduced at prolonged exposure of the polymer to irradiation. When going to extremely long irradiation times, k becomes very small and the attenuation coefficient μ will be constant along the irradiation depth direction, i.e., $\mu(x) \approx \mu_0$.

The dependence of the quantity μ_0 on the aging time t can be quantified based on a law similar to the Avrami law [35]. We chose this dependence to be of the form:

$$\mu_0 = A_2 - A_1 \exp(-Kt^n), \tag{11}$$

where K and n are Avrami-like parameters. The difference $A_2 - A_1$ corresponds to the value of μ_0 at the aging time $t = 0$. The coefficient A_2 describes the saturation value of μ_0. This equation was used to fit our experimental data, namely μ_0 versus aging time (Fig. 6a). The quality of the fit supports the Avrami-like functional dependence for the interpretation of the evolution of aging effects in NR induced by UV light with the aging time.

4. Conclusions

The aging process of cross-linked NR under the effect of UV light has been studied by ^{1}H transverse relaxation with a unilateral NMR sensor. The Profile NMR-MOUSE® provides depth resolution in the micrometer range and was found to be a unique tool for measuring of the changes induced by UV irradiation in natural rubber. An NMR observable based on the sum of initial CPMG echoes was shown to be proportional to $\overline{T}_{2\text{eff}}$ and used to build UV attenuation profiles.

The aging profiles were interpreted for the first time based on a model in which the radiation absorption coefficient depends on the depth in the sample. The parameters describing the depth dependence of the radiation attenuation coefficients are functions of the aging time. An Avrami-like equation was proposed to describe the changes in the absorption coefficient with irradiation time. Being a sensitive method for the measurement of cross-link density modifications in elastomers, NMR relaxometry with high precision mobile sensors like the profile NMR-MOUSE® can be used to quantitatively and qualitatively characterize the surface aging effects induced by different physical and chemical agents.

Acknowledgment

D.E.D. gratefully acknowledged the support of Romanian Ministry of Education and Research under Project PN II, ID-1102.

References

[1] J. Weiss, Chemical effects in the irradiation of polymers in the solid state, J. Polym. Sci. 29 (1958) 425.

[2] A.A. Miller, E.J. Lawton, J.S. Balwit, The radiation chemistry of hydrocarbon polymers: polyethylene, polymethylene and octacosane, J. Phys. Chem. 60 (1956) 599.

[3] J.F. Fowler, F.T. Farmer, Conductivity induced in unplasticized "Perspex" by X-rays, Nature 175 (1955) 516.

[4] V.E. Skurat, I.I. Dorofeev, The transformations of organic polymers during the illumination by 147 and 1236 nm light, Ang. Makrom. Chem. 216 (1994) 205.

[5] B. Blümich, NMR Imaging of Materials, Clarendon Press, Oxford, 2000.

[6] P.T. Callaghan, Principles of Nuclear Magnetic Resonance Microscopy, Clarendon Press, Oxford, 1991.

[7] R. Kimmich, NMR: Tomography, Diffusometry, Relaxometry, Springer-Verlag, Berlin, 1997.

[8] B. Blümich, D.E. Demco, NMR Imaging of Elastomers in Handbook of Spectroscopy of Rubbery Materials, in: V.M. Litvinov, P.P. De (Eds.), Rapra Technology Ltd., Shawbury, 2002.

[9] D.E. Demco, B. Blümich, Solid-state NMR imaging methods. Part I and II, Conc. Magn. Reson. 12 (2000), 188 and 269.

[10] D.E. Demco, B. Blümich, NMR imaging of materials, Curr. Opin. Solid State Mat. Sci. 5 (2001) 195.

[11] P. Blümler, B. Blümich, Aging and phase separation of elastomers investigated by NMR imaging, Macromolecules 24 (1991) 2183.

[12] A. Spyros, R. Kimmich, B.H. Briese, D. Jendrosek, ^{1}H NMR imaging study of enzymatic degradation in poly(3-hydroxybutyrate) and poly(3-hydroxybutyrate-*co*-3-hydroxyvalerate). Evidence for preferential degradation of the amorphous phase by PHB depolymerase B from *Pseudomonas lemoignei*, Macromolecules 30 (1997) 8218.

[13] M. Garbarczyk, W. Kuhn, J. Klinowski, S. Jurga, Characterization of aged nitrile rubber elastomers by NMR spectroscopy and microimaging, Polymer 43 (2002) 3169.

[14] J.A. Chudek, G. Hunter, Nuclear magnetic resonance chemical shift-selective microimaging of samples of degraded rubber hosepipe and of high-impact polystyrene, J. Mater. Sci. Lett. 4 (1992) 222.

[15] P. Barth, S. Hafner, Investigation of aging in polymer networks by $T_{1\rho}$ material property NMR imaging, Magn. Reson. Imag. 15 (1997) 107.

[16] S. Hafner, P. Barth, Aging of polymer networks as studied by material property NMR imaging, Magn. Reson. Imag. 13 (1995) 739.

[17] D.A. Low, J.F. Dempsey, R. Ventatesan, S. Mutic, J. Markman, E.M. Haacke, J.A. Purdy, Evaluation of polymer gels and MRI as a 3-D dosimeter for intensity-modulated radiation therapy, Med. Phys. 26 (1999) 1542.

[18] T.M. Alam, B.R. Cherry, K.M. Minard, M. Celina, Relaxation nuclear magnetic resonance imaging investigation of heterogeneous aging in a hydroxy-terminated polybutadiene-based elastomer, Macromolecules 38 (2005) 10694.

[19] M. Schneider, D.E. Demco, B. Blümich, NMR images of proton residual dipolar coupling from strained elastomers, Macromolecules 34 (2001) 4019.

[20] M. Schneider, D.E. Demco, B. Blümich, ^{1}H NMR imaging of residual dipolar couplings in cross-linked elastomers: dipolar-encoded longitudinal magnetization, double-quantum, and triple-quantum filters, J. Magn. Reson. 140 (1999) 432.

[21] R. Fechete, D.E. Demco, B. Blümich, Chain orientation and slow dynamics in elastomers by mixed magic-Hahn echo decays, J. Chem. Phys. 118 (2003) 2411.

[22] M. Schneider, L. Gasper, D.E. Demco, B. Blümich, Residual dipolar couplings by ^{1}H dipolar-encoded longitudinal magnetization, double- and triple-quantum nuclear magnetic resonance in cross-linked elastomers, J. Chem. Phys. 111 (1999) 402.

[23] P.J. McDonald, Stray field magnetic resonance imaging, Prog. Nucl. Magn. Res. Spectrosc. 30 (1997) 69.

[24] J. Perlo, F. Casanova, B. Blümich, Profiles with microscopic resolution by single-sided NMR, J. Magn. Reson. 176 (2005) 64.

[25] G. Eidmann, R. Savelsberg, P. Blümler, B. Blümich, The NMR MOUSE a mobile universal surface explorer, J. Magn. Reson. A 122 (1996) 104.

[26] F. Balibanu, K. Hailu, K. Eymael, D.E. Demco, B. Blümich, Nuclear magnetic resonance in inhomogeneous magnetic fields, J. Magn. Reson. 145 (2000) 246.

[27] G. Zimmer, A. Guthausen, B. Blümich, Characterization of cross-link density in technical elastomers by the NMR-MOUSE, Solid State Nucl. Magn. Reson. 12 (1998) 183.

[28] A. Guthausen, G. Zimmer, P. Blümler, B. Blümich, Analysis of polymer materials by surface NMR via the MOUSE, J. Magn. Reson. 130 (1998) 1.

[29] K. Hailu, R. Fechete, D.E. Demco, B. Blümich, Segmental anisotropy in strained elastomers detected with a portable NMR scanner, Solid State Nucl. Magn. Reson. 22 (2002) 327.

[30] M. Klein, R. Fechete, D.E. Demco, B. Blümich, Self-diffusion measurements by a constant-relaxation method in strongly inhomogeneous magnetic fields, J. Magn. Reson. 164 (2003) 310.

[31] P. Prado, B. Blümich, One-dimensional imaging with a palm-size probe, J. Magn. Reson. 144 (2000) 200.

[32] F. Casanova, B. Blümich, Two-dimensional imaging with a single-sided NMR probe, J. Magn. Reson. 163 (2003) 38.

[33] T.B. Benson, P.J. McDonald, The application of spin echoes to stray-field imaging, J. Magn. Reson. B109 (1995) 314–317.

[34] M. Schneider, L. Gasper, D.E. Demco, B. Blümich, Residual dipolar couplings by ^{1}H dipolar-encoded longitudinal magnetization, double- and triple-quantum nuclear magnetic resonance in cross-linked elastomers, J. Chem. Phys. 111 (1999) 402.

[35] M. Avrami, Kinetics of phase change. II. Transformation-time relations for random distribution of nuclei, J. Chem. Phys. 8 (1940) 212.